The field-circuit analysis of the start-up operation of the brushless DC motor

Łukasz Knypiński, Lech Nowak, Kazimierz Radziuk
Poznan University of Technology
60 – 965 Poznań, ul. Piotrowo 3a, e-mail: Lukasz.Knypinski@doctorate.put.poznan.pl,
Lech.Nowak@put.poznan.pl, Kazimierz.Radziuk@put.poznan.pl

Yvonnick Le Menach
University of Science and Technologies of Lille
Cité Scientifique, 59 655 Villeneuve d'Ascq, France
e-mail: Yvonnick.Le-menach@univ-lille1.fr

1. Introduction

Nowadays, we can observe growing concern about energy saving and the protection of natural environment. It is reflected in recent researches carried out by designers who try to find new, high, efficient machines. Therefore, development of constructions of the permanent magnet motors is being accelerated. The permanent magnet brushless DC (BLDC) motors state an important group of these types of machines. The BLDC motors have many advantages: high efficiency, high power density, wide speed range, good dynamic performance and long operational life [9, 17]. The BLDC motors are widely used in different industrial applications [1]. The further development of BLDC motors is possible owing to the development production technology and the improvement of permanent magnets parameters. Research and works connected with development of methods of simulation of transient and dynamic states in BLDC motors and advancement of optimization procedures will increase knowledge of these motors. The results of field-circuit analysis connected with optimization algorithm can show some new principle directions of the development of BLDC motor structures.

In the paper an algorithm and computer code for the analysis of the outer rotor permanent magnet brushless DC motor dynamics is presented. The mathematical model of the devices includes: the equation of a electromagnetic field, the electric circuit equations and the equation of mechanical motion. The numerical implementation is based on the finite element method (FEM) and step-by-step algorithm. The nonlinear coupled field-circuit equations have been solved by using Newton-Raphson algorithm. The electric circuits of the converter during transient operation have been discussed. The computer code for dynamic simulation of the machine has been elaborated on the basis of Delphi environment. The start-up of the motor has been investigated. Selected results of the analysis are presented and discussed.

2. Structure of the machine

The brushless DC motors consist of a permanent magnet rotor and stator equipped with a three phase winding. The construction of the considered motor is presented in Figure 1a. The inner stator has 12 slots. The three-phase concentrated non-overlapping winding has been applied [5]. In such constructions the ends of winding are shorter than in case of classical overlapping winding. As a result, lower copper losses can be achieved. The stator winding is star-connected. The winding configuration is shown in Figure 1b. As it can be seen, each phase have two coils connected in series. At each moment, there are two phases in conducting state and one phase

in non-conducting state. In the outer rotor 10 pieces of the permanent magnet are mounted. The motor is equipped with Recoma 22 ($Sm_{22}Co_{17}$) type magnets [19]. In the discussed machine, the correlation between the number of stator slots N_s and the number of pole pairs p have to satisfy relationship $2p = N_s \pm 2$ [6]. Thus, the motor has a fractional ratio of slots number to pole number. In such motors the cogging torque has lower values.

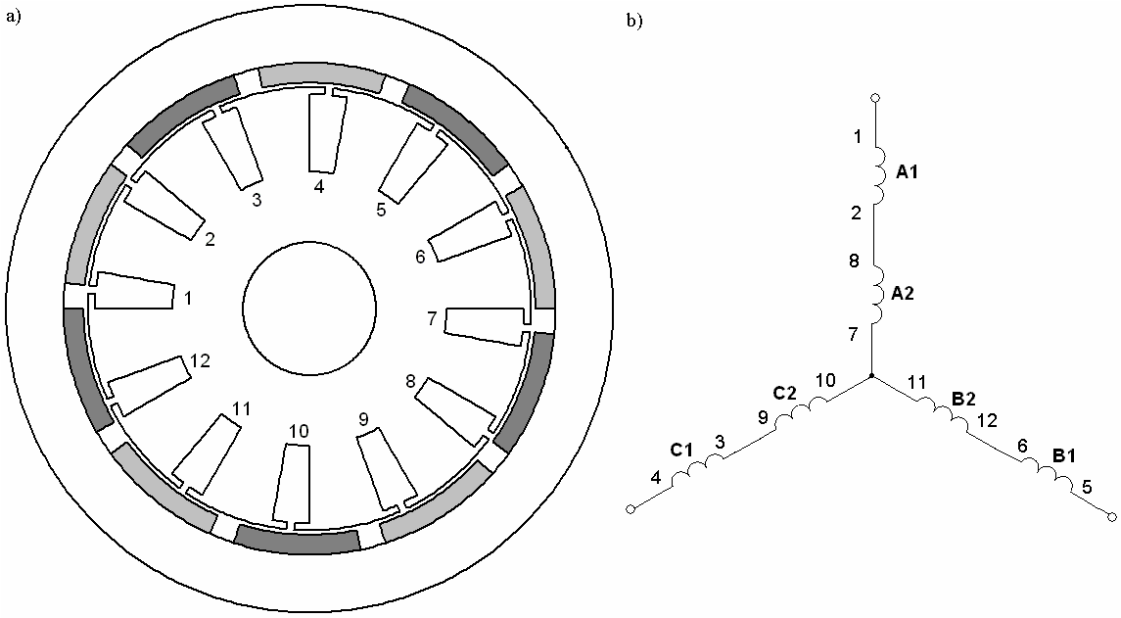

Fig. 1. The outer rotor permanent magnet brushless DC machine (a) and the stator winding configuration (b)

3. Mathematical model

In BLDC machine the magnetic field is excited by two sources: permanent magnet and stator windings. Thus, the equations describing magnetic field can be written as follows

$$\mathrm{curl}\left(\nu \mathrm{curl}\vec{A}\right) = \vec{J} + \vec{J}_M \tag{1}$$

where $\nu = \mu^{-1}$ is the magnetic reluctivity, $\vec{A}$ is the magnetic vector potential, $\vec{J}$ is the current density in windings, $\vec{J}_M = \mathrm{curl}\vec{M}$, $\vec{M}$ is the magnetization vector within the permanent magnet area.

The electric machines are generally voltage supplied. The waveforms of currents $i_1(t)$, $i_2(t)$, $i_3(t)$ in the stator windings are not known in advance, i.e. prior to the field calculation. Therefore, it is necessary to consider the voltage equations of the motor

$$\frac{\mathrm{d}\mathbf{\Psi}}{\mathrm{d}t} + \mathbf{Ri} = \mathbf{u} \tag{2}$$

where $\mathbf{\Psi}$ is the matrix of flux linkage, $\mathbf{R}$ is the diagonal matrix of winding resistances, $\mathbf{i} = [i_1\ i_2\ i_3]^T$, $\mathbf{u} = [u_1\ u_2\ u_3]^T$ are the vectors of winding currents and supply voltages, respectively.

The equation describing mechanical motion in rotary machine may be expressed as

$$J\frac{\mathrm{d}\omega}{\mathrm{d}t} = T - T_{lo} \tag{3}$$

where J – is the moment of inertia, ω – is the angular velocity of the rotor, T – is the electromagnetic torque, T_{lo} – is the load torque.

3. Coupled field-circuit implementation

In the numerical implementation of the motor transients the finite element method (FEM) and the stepping procedure have been applied. At the *n*-th time step the set of equations describing magnetic field takes the form

$$\mathbf{S}_n\mathbf{\Phi}_n = \mathbf{z}\mathbf{i}_n + \mathbf{\Theta}_{Mn} \tag{4}$$

where $\mathbf{S}_n$ is the stiffness matrix at time t_n, $\mathbf{\Phi}_n$ is the vector of nodal potentials multiplied by the machine length [4, 14], $\mathbf{z}$ is the matrix of turn numbers associated with the nodes within the windings area, $\mathbf{\Theta}_{Mn}$ is the vector of magneto-motive forces in the permanent magnets area [7, 15].

In order to solve the Kirchhoff's equations the time stepping algorithm has been employed. After substituting $\mathbf{\Psi}_n = \mathbf{z}^T\mathbf{\Phi}_n$ [11] into equation (2), the voltage equations describing the motor windings at $t = t_n$ may be expressed in the form

$$\mathbf{z}^T\mathbf{\Phi}_n - \mathbf{z}^T\mathbf{\Phi}_{n-1} + \Delta t\mathbf{R}\mathbf{i}_n = \Delta t\mathbf{u}_n \tag{5}$$

in which $\Delta t = t_n - t_{n-1}$ is the time step length.

The nonlinearity of the magnetic core has been taken into account. In this case, matrix $\mathbf{S}_n$ depends on solution $\mathbf{\Phi}_n$. In the elaborated algorithm the Newton-Raphson procedure has been applied. At the *n*-th time step and *k*-th iteration, the unknown vectors $\mathbf{\Phi}_n^k$ and $\mathbf{i}_n^k$ are replaced with their increments: $\delta\mathbf{\Phi}_n^k = \mathbf{\Phi}_n^k - \mathbf{\Phi}_n^{k-1}$ and $\delta\mathbf{i}_n^k = \mathbf{i}_n^k - \mathbf{i}_n^{k-1}$. The set of coupled field-circuit equations can be written in the form [10]

$$\begin{bmatrix} \mathbf{H}_n^k & -\mathbf{z} \\ \mathbf{z}^T & \Delta t\mathbf{R} \end{bmatrix}\begin{bmatrix} \delta\mathbf{\Phi}_n^k \\ \delta\mathbf{i}_n^k \end{bmatrix} = \begin{bmatrix} \mathbf{\Theta}_{Mn} - \mathbf{S}_n^k\mathbf{\Phi}_n^{k-1} + \mathbf{z}\mathbf{i}_n^{k-1} \\ \Delta t\mathbf{u}_n + \mathbf{z}^T\mathbf{\Phi}_{n-1} - \mathbf{z}^T\mathbf{\Phi}_n^{k-1} - \Delta t\mathbf{R}\mathbf{i}_n^{k-1} \end{bmatrix} \tag{7}$$

where $\mathbf{H}_n^k$ is the Hessian matrix of the Newton-Raphson process.

The value of Hessian matrix for *m*-th finite element is determined as follows

$$H_{i,j}^m = S_{i,j}^m + \frac{2}{(\nu^m)^2\Delta^m}\frac{\partial\nu}{\partial(B^2)}\left(\sum_{q=1}^{3} S_{i,q}^m\Phi_q\right)\left(\sum_{q=1}^{3} S_{j,q}^m\Phi_q\right) \tag{8}$$

where i, j are the nodes of triangle finite element, Δ^m is the area of *m*-th element, B is the modulus of magnetic flux density in the *m*-th element.

After solving the system (7), the vector of currents $\mathbf{i}_n^k$ and the vector of nodal potential $\mathbf{\Phi}_n^k$ can be determined. The iterative Newton-Raphson algorithm was discussed in [8].

The movement of the rotor has been modelled by means of the method of distorted elements [3]. The value of angular position of the rotor at $t = t_{n+1}$ is evaluated by explicit difference formula [3]

$$\alpha_{n+1} = (\Delta t)^2 \frac{T_n - T_{lo}}{J} + 2\alpha_n - \alpha_{n-1} \tag{9}$$

where α_n is the angular position of the rotor at the time t_n, T_n is the electromagnetic torque at $t = t_n$.

Finally the angular velocity ω of the rotor can be estimated as

$$\omega(t_n + 0.5\Delta t) = \frac{\alpha_{n+1} - \alpha_n}{\Delta t} \tag{10}$$

4. The electrical commutation

The BLDC motors do not have brushes, instead of it, there are electrically commuted. Voltage commutation is carried out by the conventional six-switch converter. The scheme of the converter, connected with motor circuit model is shown in Figure 2.

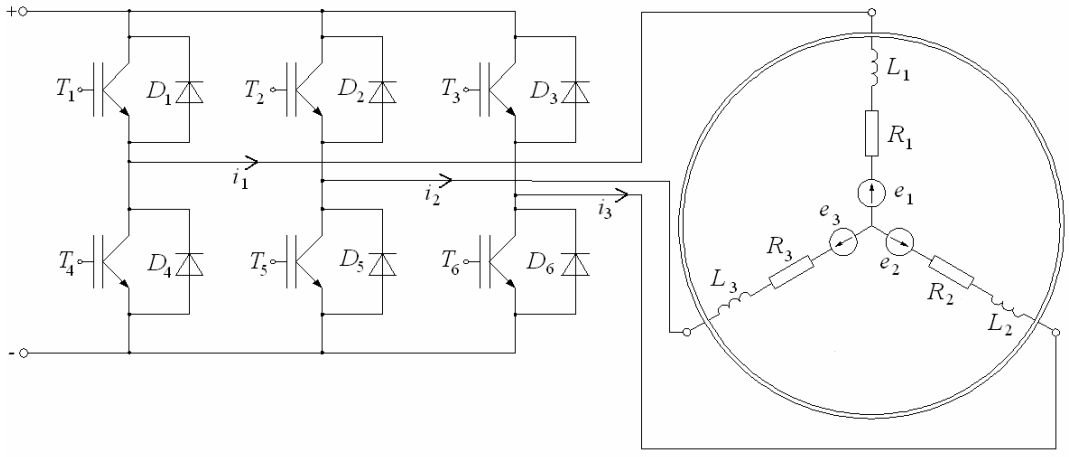

Fig. 2. The conventional six-switch converter connected with motor circuit model

The stator phase voltage equations can be described as

$$\begin{cases} u_1 = R_1 i_1 + \dfrac{\mathrm{d}\Psi_1}{\mathrm{d}t} + e_1 \\ u_2 = R_2 i_2 + \dfrac{\mathrm{d}\Psi_2}{\mathrm{d}t} + e_2 \\ u_3 = R_3 i_3 + \dfrac{\mathrm{d}\Psi_3}{\mathrm{d}t} + e_3 \end{cases} \tag{11}$$

where e_1, e_2, e_3 are the back electromotive forces in the stator windings.

In the studied motor, the stator windings are star-connected, so:

$$i_1 + i_2 + i_3 = 0 \tag{12}$$

In such motors only two phases are voltage supplied. The third phase is not powered and is short-circuited by diode when the current is different from zero. Therefore, only two voltage equations are considered. Taking into account (12) the voltage equations (11) may be expressed in the form

$$\begin{cases} u_{12} = R_1 i_1 - R_2 i_2 + \dfrac{\mathrm{d}\Psi_1}{\mathrm{d}t} - \dfrac{\mathrm{d}\Psi_2}{\mathrm{d}t} + e_1 - e_2 \\ u_{23} = (R_1 + R_3) i_2 + R_3 i_1 + \dfrac{\mathrm{d}\Psi_2}{\mathrm{d}t} - \dfrac{\mathrm{d}\Psi_3}{\mathrm{d}t} + e_2 - e_3 \end{cases} \tag{13}$$

where $u_{12} = u_1 - u_2$ and $u_{23} = u_2 - u_3$.

Switching sequence of winding depends on the rotor position. The configuration which produces the highest torque waveform has been chosen. The rotor position is usually sensed by Hall sensors [13]. These Hall sensors are put every 120˚. The sensors generate digital signals which give information about rotor position. Using three Hall sensors and conventional six-switch converter, the six different converter states are possible. In order to produce maximum torque, the converter should be commuted every 60 electric degrees. The alternative way is the sensorless method. These methods can be based on sensing currents in two phases or the determination of back electromotive forces (EMF) [2, 17].

The switching sequence of the transistor has been determined on the basis of back EMF inducted in the stator windings. The back EMF waveforms inducted in the stator winding are presented in Figure 3. The calculation have been executed for steady-state velocity equal to 504 rpm and load torque $T_{lo} = 2.5$ Nm.

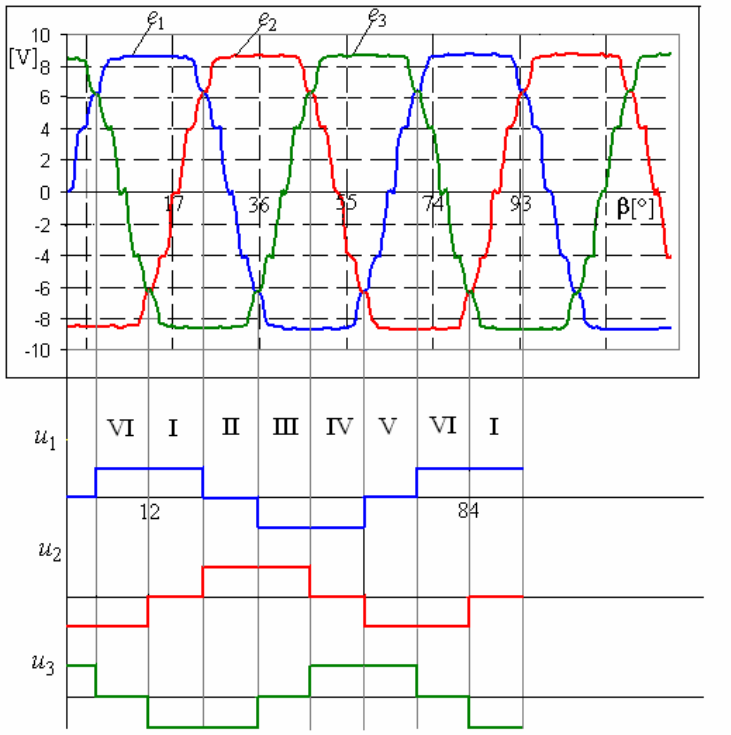

Fig. 3. Calculated back EMF and voltage waveforms of load machine

The switching sequence of the transistors and diodes, switching intervals and rotor position are listed in Table 1. The β is the mechanical angle. Switching intervals are presented in electrical degrees. As it can be noticed from Table 1, the transistors are conduct within 120 electrical degrees. The diodes conduct only when the phase current is switching off. The studied motor has 5 pairs of poles in the outer rotor. Therefore, in this case 360 electrical degrees correspond to 72 mechanical degrees. The five pole pairs BLDC motors need five electrical cycles to execute one rotation of the rotor.

Table 1. Switching sequence of the transistors and diodes of the converter

Converter state	Switching interval	Rotor position β [°]	Transistor ON	Diode ON
I	0˚ – 60˚	0 – 12	T1, T6	D2
II	60˚ – 120˚	12 – 24	T2, T6	D4
III	120˚ – 180˚	24 – 36	T2, T4	D3
IV	180˚ – 240˚	36 – 48	T3, T4	D5
V	240˚ – 300˚	48 – 60	T3, T5	D1
VI	300˚ – 360˚	60 – 72	T1, T5	D6

Figure 4 illustrates the electric connection of the stator windings and current direction in the six converter states. The numbers 1,2 and 3 indicate the motor windings.

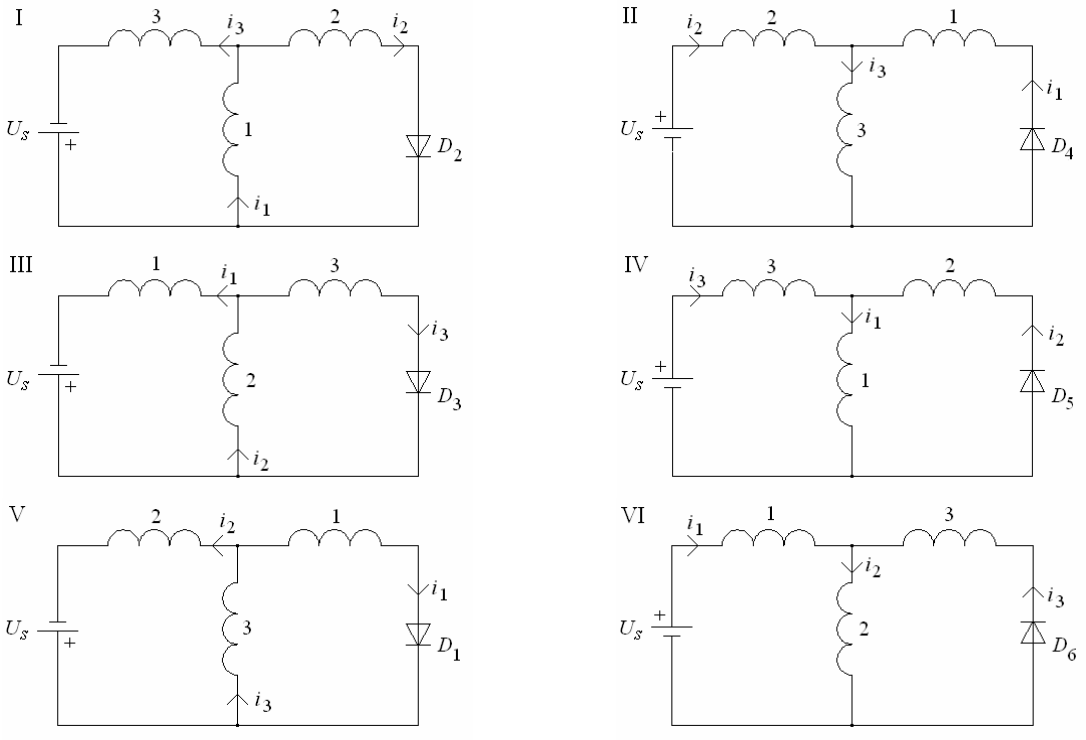

Fig. 4. The stator winding connection in the six converter states

Two current loops are considered at each of converter state. However, in each state two different periods must be studied. It has been assumed that values of voltage u_{31} and u_{12} are given. Figure 5 illustrates equivalent electric circuit of the motor in the 4-th converter state. In this case the phase 2 is not powered. In the first period – after phase commutation, the current i_2 in the switched phase 2 has value different from zero. It flows through windings 1, 2 and diode D5 (see dash dot marked current loop on Fig. 5). Then the voltages are equal to

$u_{31} = U_s + e_1 - e_3$ and $u_{12} = e_2 - e_1$. When the current i_2 achieves zero, the currents $i_3 = -i_1$ and voltages $u_{31} = U_s + e_1 - e_3$ and $u_{12} = -0.5(U_s + e_1 - e_3)$.

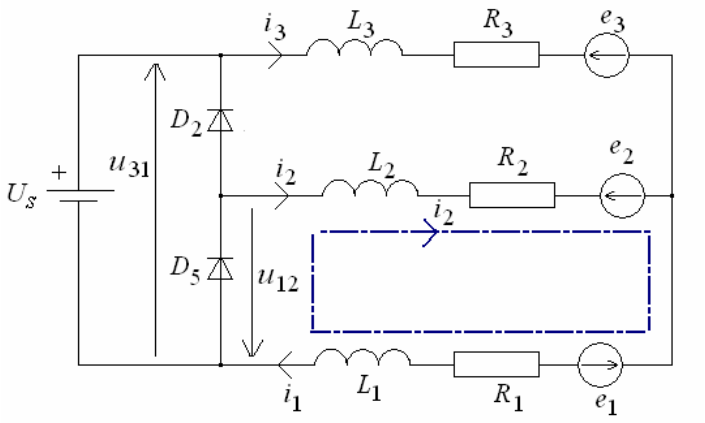

Fig. 5. The equivalent electric circuit for IV stage of converter

5. The simulation of the dynamics

In this section the dynamic operation, i.e. operation with unknown varying angular velocity is investigated. In order to solve transient dynamics state, the field-circuit model (7) has been applied. Additionally, the equations describing mechanical motion (9) and (10) have been included into mathematical model of the motor. The algorithm and the computer code for simulation of the motor dynamics have been developed. The start-up of the loaded permanent magnet brushless DC motor with outer rotor has been studied. The cross section of the motor has been subdivided into 10080 triangular elements. Such number of elements ensure sufficient precision of the simulation. The switching sequence of the converter transistors has been elaborated on the basis of back electromotive forces in the stator winding and rotor position – see section 4. The motor has been controlled by using the switching algorithm presented in Table 1. The calculations have been performed for $J = 0.002$ kgm^2, $T_{lo} = 2.0$ Nm, $\Delta t = 0.334$ ms and supply voltage equal to $U_S = 24$ V. In order to calculate angular velocity, electromagnetic torque, back electromotive forces and currents waveforms, the coupled field-circuit non-linear and motion equations have been solved simultaneously with Newton-Raphson process. The waveforms of back EMF are shown in Figure 6.

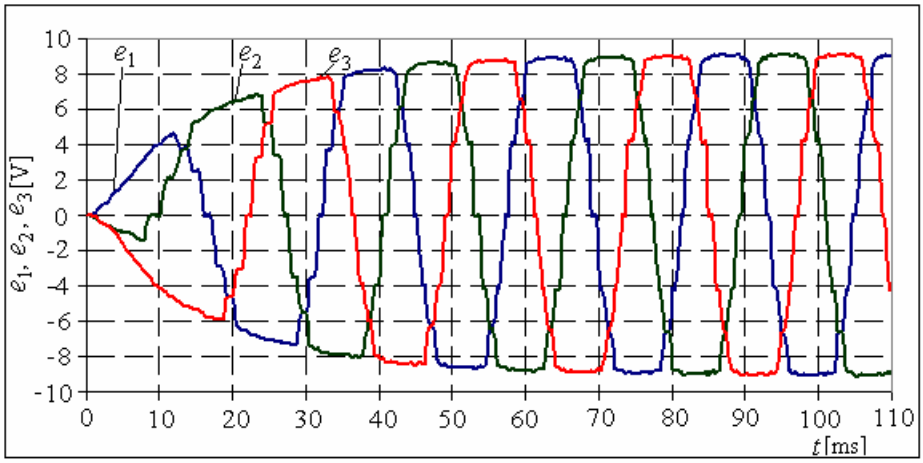

Fig. 6. Back EMF waveform

As it can be seen from Figure 6, the maximum values of EMF are equal to $e_1 = e_2 = e_3 \cong 9.05$ V when the velocity achieve approximately steady-state value 510 rpm. The waveforms of windings currents, angular velocity and electromagnetic torque are shown in Figures 7, 8, 9 and 8 respectively.

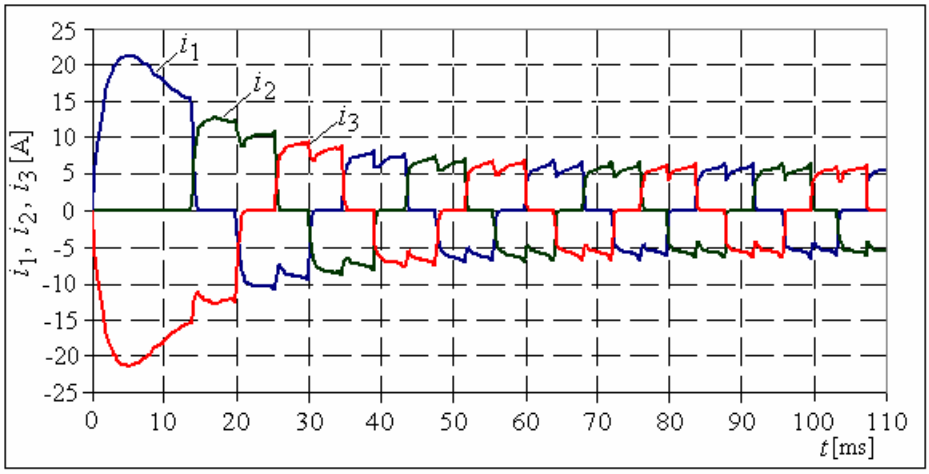

Fig. 7. Phase current waveforms

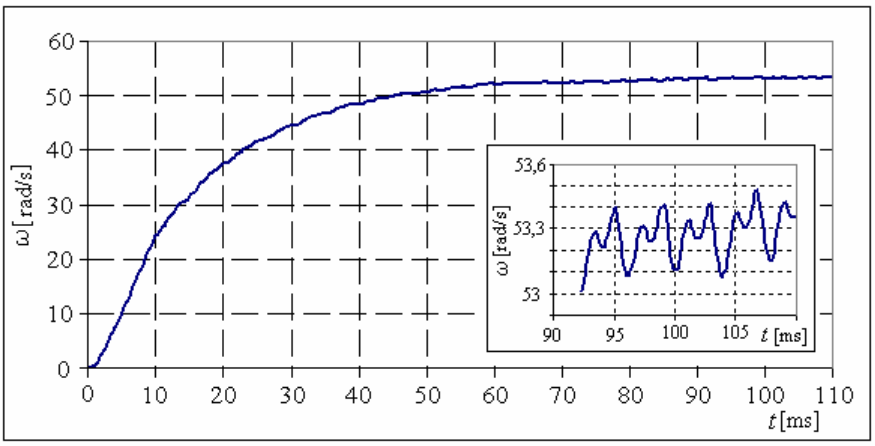

Fig. 8. Angular velocity waveform

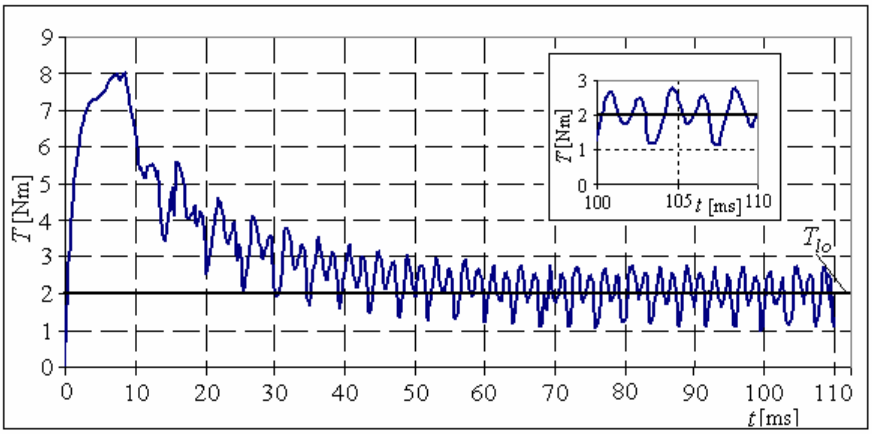

Fig. 9. Torque waveform

As it can be noticed from the figures, the maximum values of torque $T = 8$ Nm and currents $I_1 = -I_2 = 21.22$ A have been obtained.

In the torque waveform (Figure 10), and as well as in the velocity waveform (Figure 8) substantial oscillations can be observed. They are caused by cogging torque and converter commutation [19]. The cogging torque is generated by interactions between permanent magnets and stator teeth. The shape of cogging torque waveform depends on machine's structure [14]. The reduction of this oscillations may be obtained by the optimization of machine magnetic circuit geometry. On the other hand, the examined BLDC motor is controlled by conventional six-switch converter. The phase commutation depends on the rotor position. The converter also produces oscillations in the torque waveform. These oscillations are caused by change of currents direction in the stator winding. In order to reduce such torque ripple, a RC filter connected with the input of the motor can be applied [12]. When we study BLDC motor connected with converter, it is necessary to optimize the motor geometry and the control system parameters at the same time.

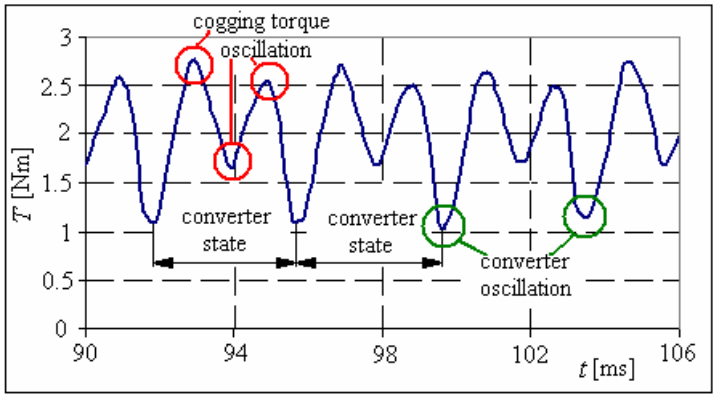

Fig. 10. Oscillations in torque waveform

6. Conclusions

The elaborated algorithm and the software can be successfully applied in the simulation of BLDC motors dynamics. The algorithm has been tested. It has a good convergence and is very efficient. Due to the parameterization, different structures of BLDC motors can be simulated. The algorithm can be supplemented with non-deterministic optimization procedure in the nearest future. After that, the authors want to complete the three optimization tasks. In the first one, the optimization of the geometry of the selected motor will be executed. In the second one, the parameters of supply and control system will be optimized. In the third one, the complex optimization of the motor geometry and control system will be carried out.

Acknowledgment

This work has been financially supported by the project No. POIG.01.01.02-00-113/09

References

[1] Chen J., Guo Y., Zhu J., Development of a high-speed permanent-magnet brushless DC motor for driving embroidery machines, IEEE Transactions on Magnetics, vol. 43, No. 11, pp. 4004 – 4009, 2007.

[2] Dixon J., W., Rodríguez M., Huerta R., Simplified Sensorless Control for BLDC Motor, The 19th International Battery, Hybrid and Fuel Cell Electric Vehicle Symposium EVS-19, Busan, South Korea, pp. 1432 – 1442, 2002.

[3] Demenko A., Nowak L., Szelag W., Numerical formulation of motion equation in dynamic finite element analysis of electromechanical converters, Proceedings of International Workshop "Electric and Magnetic Fields", Liege, Belgium, 28 - 30 September1992, pp. 610 – 616.
[4] Demenko A., Sykulski J., Wojciechowski R., Network representation of conducting regions in 3-D finite elements descriptions of electrical machines, IEEE Transactions on Magnetics, vol. 44, No. 6, pp. 714 – 717, 2008.
[5] Ishak D., Zhu Z. Q., Howe D. 2005, Permanent-magnet brushless machines with unequal tooth widths and similar slot and pole number, IEEE Transactions on Industry Applications, vol. 41, No. 2, pp. 584 – 590, 2005.
[6] Ishak D., Zhu Z. Q., Howe D., Comparative study of permanent magnet brushless motors with all teeth and alternative teeth windings, Proceedings of IEE 2nd International Conference Power Electronic, Machines and Drives, pp. 834-839, 2004.
[7] Knypiński Ł., The steady-state and transient FEM analysis of the outer-rotor permanent magnet brushless DC motor, Proceedings of X International PhD Workshop OWD 2008, Wisla, Poland, pp. 277 – 280.
[8] Knypiński Ł., Nowak L., Fidel-circuit simulation of the outer rotor permanent magnet brushless DC motor taking nonlinearity into account, Proceedings of XIV International Symposium on Electromagnetic Fields in Mechatronics, Electrical and Electronic Engineering ISEF 2009, Arras, pp. 247 – 248.
[9] Lindth P. M., Jussila H. K., Niemelä M., Parviainen A., Pyrhönen J., Comparison of concentrated windings permanent magnet motors with embedded and surface mounted rotor magnets, IEEE Transactions on Magnetics, vol. 45, No. 5, pp. 2085 – 2089, 2009.
[10] Nowak L., Dynamic operation of an electromagnetic actuator taking nonlinearity and eddy currents into account, COMPEL, vol. 18, No. 4, pp. 611 – 618, 1999.
[11] Nowak L., Radziuk K., Transient analysis of PWM-excited electromagnetic actuators, IEE Proceedings-Science, Measurement and Technology, Vol. 149, 2002, pp. 199 – 202.
[12] Rajan A. A., Vasantharatha S., Harmonics and torque ripple minimization using L-C filter for brushless DC motors, International Journal of Recent Trends in Engineering, vol. 2, No. 5, pp. 239 – 243, 2009.
[13] Samaylenko N., Han Q., Jatskevich J., Dynamics performance of brushless DC motors with unbalanced Hall sensors, IEEE Transactions on Energy Conversion, vol. 23, No. 3, pp. 752 – 763, 2008.
[14] Saied S. A., Abbaszadeh K., Hemmati S., Fadaie M., A new approach to cogging torque reduction in surface-mounted permanent-magnet motors, European Journal of Scientific Research, vol. 26, No. 4, pp. 499 – 599, 2009.
[15] Stachowiak D., Edge element analysis of brushless motors with inhomogeneously magnetized permanent magnets, COMPEL, vol. 23, No. 4, pp. 1119 – 1128, 2004.
[16] Szeląg W., Numerical method of calculation of magnetic field distribution in synchronous machine, Academic Journals of Poznan University of Technology, No. 37, 1989.
[17] Shao J., Nolan D., Teissier M., Swanson D., A novel microcontrotroller-based sensorless brushless DC (BLDC) motor drive for automotive fuel pumps, 37 th Industry Applications Annual Meeting IAS'02, Pittsbourgh, vol. 4, pp. 2386 – 2392, 2002.
[18] Yong Wang, Chau K. T., Chan C., C., Jiang J. Z., Transient analysis of a new outer-rotor permanent-magnet brushless DC motor drive using circuit-field-torque coupled time-stepping finite-element-method, IEEE Transactions on Magnetics, vol. 38, No. 2, pp. 1297 – 1300, 2002.
[19] Yong Liu, Zhu Z., Q., Howe D., Commutation-torque-ripple minimization in direct-torque controlled PM brushless DC drives, IEEE Transactions on Industry Applications, vol. 43, No. 3, pp. 1012 – 1021, 2007.
[20] http://www.arnoldmagnetics.com, July 2010.